Amplitude combinations in the critical binary fluid nitrobenzene and *n*-hexane

G. Zalczer, A. Bourgou,* and D. Beysens
Service de Physique du Solide et de Resonance Magnetique CEN-Saclay, 91191 Gif-sur-Yvette Cedex, France
(Received 14 June 1982)

We have determined experimentally the amplitudes of the correlation length and susceptibility along the three principal trajectories: critical isochore, coexistence curve, and, for the first time in a critical mixture, critical isotherm. We have also determined the amplitude of the coexistence curve and that of the specific heat along the critical isochore. These amplitudes allowed us to compute several universal amplitude combinations, which are all in agreement with current theoretical predictions, except C^+/C^- which agrees better with the renormalization-group value than with the high-temperature-series one. Moreover, linewidth measurements allowed us to determine the dynamic constant R, found to be close to unity.

I. INTRODUCTION

The hypothesis of universality has played a central role in the study of phase transitions. It arises from the fact that characteristic lengths near a critical point are much larger than the microscopic interaction scale. Therefore, these details are forgotten and most of the observed quantities depend only on the dimensionalities of the space (d) and of the order parameter (n). For instance, the three-dimensional Ising model and the fluid and binary mixtures transitions belong to the same class of universality $d=3$, $n=1$. At the present state of the theory, the exponents are universal and related by the so-called scaling laws, while the microscopic nature of the system is reflected through two independent amplitudes, at least asymptotically close to the critical point. The other amplitudes can then be deduced using universal amplitude combinations.

While the exponents and the relations between them have been subjects of experiments for a long time, the amplitudes received attention only recently. The reason for that is that their study requires the gathering of results of different kinds of experiments and therefore the knowledge of many parameters, including the critical exponents themselves. These exponents are now well known and the theoretical methods which have therefore proved their reliability can be used to calculate these new constants.

A complete check of the theory, however, requires experimental determinations of these combinations. The purpose of the present paper is to determine some of these constants for the mixture of nitrobenzene and *n*-hexane. The different techniques involved are static and dynamic light scattering (self-beating spectroscopy and Fabry-Perot interferometry), interferometry, refractometry, and volumetry. However, the measurements have been performed using the very same cell whenever possible.

Although the theory predicts the behavior of a system along the three basic trajectories (critical isochore, critical isotherm, and coexistence curve), most of the experiments so far have been limited to the critical isochore. However, in this paper, all these three trajectories will be studied.

II. THEORETICAL BACKGROUND

A. General

According to the standard terminology, we shall call M the order parameter, H the conjugate field, T_c the critical temperature, and $t=(T-T_c)/T_c$ the reduced temperature. Along the critical isochore ($t>0, M=H=0$) the following quantities will behave as follows:

susceptibility

$$\chi=\left[\frac{\partial M}{\partial H}\right]_T=C^+t^{-\gamma}/k_BT_c\ , \tag{1}$$

specific heat

$$C_p=\frac{A^+}{\alpha}k_Bt^{-\alpha}+\cdots \tag{2}$$

(where the ellipsis stands for regular part),
correlation length

$$\xi = \xi_0^+ t^{-\nu} . \tag{3}$$

Along the critical isotherm ($t=0$), whose equation is

$$H = DM^{\delta} , \tag{4}$$

we have

$$k_B T\chi = C_c H^{-\gamma/\beta\delta} \equiv \frac{1}{\delta D^{1/\delta}} H^{-\gamma/\beta\delta} , \tag{5}$$

$$\xi = \xi_0^c H^{-\nu/\beta\delta} . \tag{6}$$

Along the coexistence curve ($H=0, t<0$), whose equation is

$$M = B(-t)^{\beta} , \tag{7}$$

we have

$$k_B T\chi = C^-(-t)^{-\gamma} , \tag{8}$$

$$C_p = k_B \frac{A^-}{\alpha}(-t)^{-\alpha} + \cdots \tag{9}$$

(where the ellipsis again represents regular part),

$$\xi = \xi_0^-(-t)^{-\nu} . \tag{10}$$

All these formulas hold asymptotically close to the critical point. Further away, multiplicative corrective factors of the form

$$(1 + at^{\Delta} + \cdots) \tag{11}$$

must be introduced.[1]

The values admitted now for the exponents are[2] $\gamma=1.240$, $\nu=0.630$, $\alpha=0.110$, $\beta=0.325$, $\delta=4.815$, and $\Delta=0.50$, and we expect the combinations reported in Table I to be universal. We shall now consider the experimental determinations of the quantities involved.

B. Order parameter and coexistence curve

We have deliberately chosen magnetic notations to stress an important problem. The exact order parameter is not known in the case of binary fluids (it might be mass fraction or volume fraction or. . .) as well as in pure fluids. This is of little importance as far as only exponents are of interest but it makes it impossible to assign an amplitude to the order parameter or to the susceptibility without introducing an arbitrary factor. This factor cancels out in the final relations but one has to take care of using coherent conventions throughout. In fact, any quantity linear in the concentration can be used as a "practical" order parameter. We must therefore keep in mind which parameter we use. This arbitrary choice will not, however, affect the value of the amplitude combinations defined above. If we

TABLE I. The expected universal amplitude combinations, their theoretical values and the experimental values determined for the nitrobenzene—*n*-hexane mixture.

Universal combination	RG value	HTS value	Experimental value (this work)
$\frac{C^+}{C^-}$	4.5[a]	5.03[b]	4.3±0.3
$\frac{\xi_0^+}{\xi_0^-}$	1.91[a]	1.96[b]	1.9±0.2
$R_c^+ = \frac{A^+C^+}{B^2}$	0.066[c]	0.059[c]	0.050±0.015
$R_\xi^+ = \xi_0^+ A^{+1/3}$	0.27[d]	0.25[e]	0.27±0.03
$R_\xi^+ R_c^{+-1/3} = \xi_0^+ \left[\frac{B^2}{C^+}\right]^{1/3}$	0.67	0.65	0.73±0.05
$R_\chi^+ = C^+ D B^{\delta-1}$	1.7[a]		1.75±0.30
$Q_2 = \frac{C^+}{C_C}\left[\frac{\xi_0^C}{\xi_0^+}\right]^{2-\eta}$		1.21[b]	1.1±0.30

[a]Reference 3.
[b]Reference 4.
[c]Reference 5.
[d]Reference 6.
[e]Reference 7.

choose the volume fraction φ, we shall define

$$B_\varphi = \frac{1}{2}\lim_{t\to 0}(\varphi_1-\varphi_2)\,|\,t\,|^{-\beta} = B\left[\frac{\partial\varphi}{\partial M}\right]_T . \tag{12}$$

C. Susceptibility

The conjugate field is the proper chemical potential difference (μ) of the components and $\chi=(\partial c/\partial\mu)_{p,T}$. However, a chemical potential is not directly measurable and one has to deduce the susceptibility from the mean square of the order-parameter fluctuations. This can be readily done by optical means, at the expense of several additional parameters, among them the coupling factor between the refractive index and the concentration fluctuations. This factor is known not to be the bulk derivative, as assumed in the Einstein theory. Indeed, we can calculate the increase of polarizability due to a fluctuation which is directly related to the bulk derivative, but there is no universally accepted formula for the scattered electric field. For a discussion of this point see, e.g., Ref. 8. But this correction is obviously independent of the nature of the fluctuation. Hence the following scheme, already used in Ref. 9. (i) Find a fluctuation that couples with light and whose absolute amplitude or related susceptibility is known. (Practically, this is the Brillouin doublet.) (ii) Record both lines at the same time, in identical geometrical conditions but in a way they can be separated (Rayleigh-Brillouin spectrum). (iii) Determine the bulk derivatives.

This eliminates systematic errors but involves many parameters, so that the final statistical uncertainty cannot be expected to be small. When Rayleigh-Brillouin spectra are not available, one can determine one amplitude for each form of the Rayleigh factor. This allows comparisons between different mixtures but not directly with theory.

The light scattered at a transfer wave vector $\vec{q}$ by a liquid mixture consists of three contributions (neglecting Raman, etc.) from the three independently decaying thermodynamic parameters: concentration φ, entropy S, and pressure p, with the intensities (omitting geometrical factors)

$$I_i(q) = I_0\frac{\pi^2}{\lambda_0^4}S_n^2\left[\frac{\partial n^2}{\partial i}\right]^2 G_i(q)\chi_i k_B T , \tag{13}$$

where λ_0 is the light wavelength in vacuum, $\partial n^2/\partial i$ the bulk derivative of the squared refractive index relative to the variable i, and χ_i the susceptibility associated with the variable i. Therefore $k_BT\chi_i$ is the amplitude of the thermal fluctuations of the parameter i. The coupling of this fluctuation with light is expressed by the factors $S_n^2(\partial n^2/\partial i)^2$, where S_n is unknown but is a function of n only. $G_i(q)$ is the interference term and is the Fourier transform of the normalized correlation function of the variable i. Except for the concentration fluctuations close to the critical point, $G_i(q)$ is equal to unity (see below). Therefore, far enough from the critical point, the ratio of two lines can be written as

$$\frac{I_i}{I_j} = \frac{\left[\frac{\partial n^2}{\partial i}\right]^2}{\left[\frac{\partial n^2}{\partial j}\right]^2}\frac{\chi_i}{\chi_j} . \tag{14}$$

The intensity of the entropy line is quite negligible in this mixture compared to that of the concentration one, which can be confounded with the whole Rayleigh peak. We therefore have

$$\frac{I_R}{2I_B} = \frac{\left[\frac{\partial n^2}{\partial\varphi}\right]^2\left[\frac{\partial\varphi}{\partial M}\right]^2\left[\frac{\partial M}{\partial H}\right]_T}{\left[\frac{\partial n^2}{\partial\rho}\right]^2\rho\left[\frac{\partial p}{\partial\rho}\right]_{s,\varphi}} . \tag{15}$$

Using the formulas

$$\left[\frac{\partial n^2}{\partial p}\right]_s = \left[\frac{\partial n^2}{\partial\rho}\right]\left[\frac{\partial\rho}{\partial p}\right]_s = 2n\left[\frac{\partial n}{\partial T}\right]_p\left[\frac{\partial T}{\partial\rho}\right]_p\left[\frac{\partial\rho}{\partial p}\right]_s \tag{16}$$

and

$$\frac{1}{\rho}\left[\frac{\partial\rho}{\partial p}\right]_s = \frac{1}{\rho v^2} , \tag{17}$$

where v is the sound velocity, we get

$$\frac{I_R}{2I_B} = \frac{\left[\frac{\partial n}{\partial\varphi}\right]^2}{\left[\frac{\partial n}{\partial T}\right]^2}\left[\frac{1}{\rho}\left[\frac{\partial\rho}{\partial T}\right]\right]^2\rho v^2\frac{C^+t^{-\gamma}}{k_BT_c}\left[\frac{\partial\varphi}{\partial M}\right]^2 . \tag{18}$$

If we define

$$C_\varphi^+ = C^+\left[\frac{\partial\varphi}{\partial M}\right]^2 , \tag{19}$$

we can notice that

$$\frac{C^+}{B^2}=\frac{C_\varphi^+}{B_\varphi^2} \tag{20}$$

and therefore the choice of the order parameter does not change the value of R_c^+.

D. Specific heat

Direct specific-heat measurements cannot be performed very near a critical point because of the contradictory requirements on the temperature jump which must be much smaller than the temperature difference to T_c but large enough to allow significant measurements. On the other hand, the weakness of the exponent and the importance of the background make the measurements very close to T_c compulsory. We can make an indirect determination, however, by separating the thermodynamic formula

$$C_{p,M}-C_{V,M}=\alpha_p V T_c\left[\frac{\partial T_c}{\partial p}\right]^{-1}$$

with

$$\alpha_p=\frac{1}{V}\left[\frac{\partial V}{\partial T}\right]_{p,M} \tag{21}$$

into regular and critical parts; hence,

$$C_{p,M}^{\text{crit}}=VT_c\left[\frac{\partial T_c}{\partial p}\right]^{-1}\alpha_p^{\text{crit}}\ . \tag{22}$$

The thermal dilatation coefficient is directly derived from density measurements. These can be performed either by volumetric methods or through refractive index determination, the latter method affording much better performances.[10] It is a little less direct because the refractive index anomaly arises, in principle, not only from the density anomaly but also from the fluctuations. Two contributions are expected.[11] One is in $t^{-\nu}$ and was demonstrated to be negligible through flow birefringence measurements.[12] The other is unfortunately also in $t^{-\alpha}$ and only the cross check of both methods, as in Appendix C, allows us to estimate it as negligible.

E. Correlation length

The correlation length appears in two different processes, one static and one dynamic. The static scattered intensity is directly related to the Fourier transform $G(k,\xi)$ of the correlation function. The determination of ξ can be performed by varying either the scattering wave vector or the temperature. The same information can also be obtained in an experimentally simpler way through turbidity measurements[13] (the integral over angles of the scattered intensity). A quantitative measurement of ξ requires a precise knowledge of the correlation function which has been available only recently.[14]

The linewidth of the order-parameter fluctuation is also a function of ξ. The previously admitted function was obtained by Kawasaki,[15,16] using mode-coupling techniques:

$$\Gamma(k,\xi)=R\frac{k_BT}{6\pi\eta\xi}k^2\Omega_K(k,\xi)\ , \tag{23}$$

where η is the shear viscosity and, using $x=k\xi$,

$$\Omega_K(x)=\frac{3}{4}\frac{1}{x^2}\left[1+x^2+\left[x^3-\frac{1}{x}\right]\tan^{-1}x\right]\ . \tag{24}$$

Originally the parameter R was believed to be unity. The value $R=1.2$ was then proposed (renormalization-group theory)[17] and some experimental data agree better with the former[18] or the latter[19] value.

Very recently, using a fixed dimension RG calculation, Paladin and Peliti[20] proposed the modified version:

$$\Omega_{PP}(x)=(x^2+1)^{x_\eta-\eta/2}[\Omega_K(x)]^{1-x_\eta-\eta}\ , \tag{25}$$

where $x_\eta=y_\eta/\nu=0.0635$ and with $R=1.075$.

III. EXPERIMENTAL REMARKS

For sake of clarity, the experimental details have been deferred to the appendixes. Even then they will be only sketched since most of them have already been described in other publications. The point we want to stress here is that all the measurements have been performed using the very same sample, except for those at varying concentration and for volume measurements, which could, however, be calibrated by comparison with the reference cell.

Indeed, the amplitudes have often been seen to be strongly dependent on impurities, and it is sometimes difficult to match the amplitudes measured in different laboratories.

This sample was in a quartz cell, sealed under

vacuum, of cylindrical shape with an inner length of 20.0 mm and an internal diameter of 18 mm. The liquids were of spectroscopic grade and filtered through 0.2-μm Teflon filters. The experimental concentration was 0.509 ± 0.002 weight fraction of nitrobenzene. It turned out in the study of the coexistence curve that the critical concentration was rather 0.525 ± 0.005. This difference clearly does not affect the measurements in the diphasic region and those above the critical point only in a very small temperature range, which can be estimated as

$$T_c\left[\frac{M}{B}\right]^{1/\beta}\simeq 2\times 10^{-3}\ \mathrm{K}\ .$$

Therefore, all data closer than ~ 10 mK had to be removed; they moreover showed systematic discrepancies with respect to current behaviors (see Appendix D).

IV. AMPLITUDE COMBINATIONS

We have determined in the appendixes

$$B_\varphi=0.77\pm0.02\ ,$$
$$C_\varphi^+=(2.8\pm0.4)\times10^{-29}\ \mathrm{m}^3\ ,$$
$$A^+=(1.05\pm0.15)\times10^{27}\ \mathrm{m}^{-3}\ ,$$
$$S_n^2C_\varphi^+=(2.45\pm0.04)\times10^{-29}\ \mathrm{m}^3\ ,$$
$$S_n^2C_\varphi^-=(0.57\pm0.02)\times10^{-29}\ \mathrm{m}^3\ ,$$
$$\xi_0^+=(2.65\pm0.07)\times10^{-10}\ \mathrm{m}\ ,$$
$$\xi_0^-=(1.4\pm0.1)\times10^{-10}\ \mathrm{m}\ ,$$
$$S_n^2(\delta DB^{\delta-1})^{-1}=(0.29\pm0.05)\times10^{-29}\ \mathrm{m}^3\ ,$$
$$\xi_0^c(BD^{1/\delta})^{-\nu/\beta}=(0.93\pm0.10)\times10^{-10}\ \mathrm{m}\ .$$

Hence, we can determine the values reported in Table I. It should be noticed first that the difference between both theoretical values is usually smaller than the uncertainty on the experimental value. Therefore we are not able to claim that one theoretical approach is in better agreement than the other. The only exception is the ratio C^+/C^- where the renormalization-group (RG) value agrees significantly better with our data.

The large uncertainty on the amplitude A^+ led us to construct the combination $R_\xi^+R_c^{-1/3}$ which is free of this variable to have a closer check of the fit between theory and experiment. Except for the exception quoted above, the difference between the theoretical and experimental value is hardly bigger than one experimental standard deviation in the worst cases. We consider this as fairly convincing evidence of the accuracy of these theories.

We have also determined the value of the dynamical constant

$$R_K=0.99\pm0.05$$

or

$$R_{PP}=0.98\pm0.05$$

according to whether we use the Kawasaki or Peliti-Paladin formulations. This value is in good agreement with the original mode-coupling prediction and disagrees with the renormalization-group one (1.20).

The comparison of the Rayleigh-Brillouin and turbidity measurements also allows the determination of the light-scattering prefactor S_n. The most widely used forms for this factor are the following:

Einstein

$$S_n=1\ ,$$

Yvon-Vuks

$$S_n=\frac{9_n^2}{(n^2+2)(2n^2+1)}=0.89\ ,$$

Rocard

$$S_n=\frac{3}{n^2+2}=0.73\ ,$$

while we get $S_n=0.94\pm0.08$, about midway between Einstein's and Yvon's values. This value also enables us to determine the amplitude of the critical isotherm

$$D=(1.70\pm0.7)\times10^{28}\ \mathrm{m}^{-3}\ .$$

V. CONCLUSION

We have determined experimentally the amplitude of the susceptibility and correlation length along the three principal trajectories of the phase diagram: critical isochore, coexistence curve, and critical isotherm. As far as we know, no data on the critical isotherm has even been obtained previously. We have also determined the amplitude of the coexistence curve and that of the specific heat along the critical isochore. These amplitudes allowed us to compute universal amplitude combinations. The experimental values are all in agreement with the renormalizaton group theoretical predictions. Except for the combination C^+/C^- they are

also in agreement with the high-temperature-series ones. Moreover, we have performed linewidth measurements along the critical isochore which allowed us to determine the dynamic constant R, found to be close to unity, in agreement with the original mode-coupling theory and in disagreement with the present renormalization-group theory. Let us recall finally that all the measurements have been performed in a single cell or recalibrated according to that cell so that drifts associated with impurities should be minimized.

APPENDIX A: COEXISTENCE CURVE

1. Method

Determining the coexistence curve of a mixture using a single sealed cell involves measuring at different temperatures a parameter directly related to the concentration in each phase. As already noted, the refractive index is an obvious choice for such a parameter. We choose a refractometric method, rather than an interferometric one because very high accuracy was not needed and because it is much easier to use when absolute values are desired. The cylindrical shape of the cell and the necessity to investigate both phases dictated the setup (Fig. 1). Two thin parallel light beams are sent through the cylindrical lens made by the cell. The image of the focus is made on a remote screen by a lens placed on a translation stage. The position of this lens allows one to determine the focus and therefore the refractive index of the fluid in the cell, at the level of the beams. The cell is immersed in a thermostatic water bath (stability 1 mK) and mounted on a vertical translation stage which allows the investigation of both phases. The absolute accuracy on a single measurement is only about $\Delta n \sim 0.01$ because the distances were difficult to measure accurately. However, a single point calibration (mixture just above the critical point, see below) allows us to gain one order of magnitude. Moreover, the differences between two measurements is limited only by the uncertainty on the position setting, which corresponds to $\Delta n \simeq 4\times 10^{-4}$. The refractive index was measured in each phase at different heights and no significant gradients have been observed.

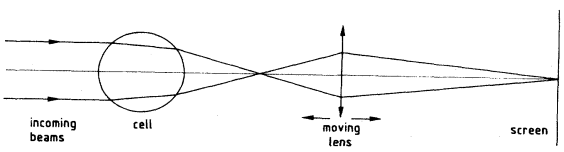

FIG. 1. Schematic representation of the setup used for measuring the refractive index of the mixture. The cell can be moved vertically in order to investigate both phases.

2. Results

The refractive index data are given in Table II. A first evidence is that the cell is not exactly at the critical concentration. Indeed the meniscus appeared near the bottom of the cell. From the extrapolation of the diameter, we can deduce a more accurate value of the critical volume fraction 0.377 instead of 0.363.[21] The critical temperature is therefore ~ 2 mK higher than the phase-separation temperature.

The difference data have been fitted allowing the critical temperature to vary within 0.01 K. A first fit, to a single power law with a fixed exponent,

$$n_1 - n_2 = 2B_n \mid t \mid^{0.325}$$

showed a systematic distortion. A corrective factor $(1+a \mid t \mid^{0.5})$ greatly improved the agreement with only a small change in B_n (Fig. 2). Further improvements of the function such as linear or 2β-power terms are therefore meaningless, though not excluded in principle. The residuals of the fit are

TABLE II. Difference of refractive indices of the two phases below T_c.

$\mid t \mid$	Δn (10^4)
1.1×10^{-4}	156
2.0×10^{-4}	194
2.8×10^{-4}	215
4.5×10^{-4}	245
4.85×10^{-4}	243
7.0×10^{-4}	271
1.1×10^{-3}	316
1.62×10^{-3}	351
2.02×10^{-3}	380
2.82×10^{-3}	416
3.82×10^{-3}	472
3.89×10^{-3}	477
4.66×10^{-3}	495
6.17×10^{-3}	546
8.16×10^{-3}	610
1.11×10^{-2}	680
1.47×10^{-2}	745
1.84×10^{-2}	802

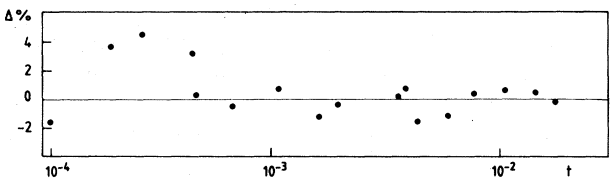

FIG. 2. Residuals of the fit of the refractive index difference data with the function $n_1-n_2=B_n\,|\,t\,|^{0.325}[1+a\,|\,t\,|^{0.5}]$ with $B_n=0.140$ and $a=3.3$.

reported in Fig. 2. The retained value is

$$B_n=0.140\pm0.002\ .$$

We have also measured the refractive index for different volume fractions at 22 °C and 5890 Å, using an Abbe refractometer (Table III). The data can be fitted by

$$n=1.3741+0.1989\varphi-0.0214\varphi^2$$

which leads to

$$\left[\frac{\partial n}{\partial\varphi}\right]_{T,p}=0.183\pm0.002\ .$$

Hence we get

$$B_\varphi=0.77\pm0.02\ .$$

3. Literature

The data of Ref. 22 have also been analyzed[23] and, when fitted to the same formula, give $\phi_c=0.377$, $T_c=19.06$ °C, $B\varphi=0.767$, $a=0.61$, and are therefore in excellent agreement with our result.

TABLE III. Refractive index data above T_c vs the volume fraction of nitrobenzene (NBZ). They can be represented by the function $n=1.3741+0.1989\varphi-0.0214\varphi^2$.

$n\left[\begin{matrix}5890\text{ Å}\\22\text{ °C}\end{matrix}\right]\pm5\times10^{-4}$	φ_{NBZ}
1.3741	0
1.4213	25
1.4326	30
1.4427	35
1.4488	40
1.4593	45
1.4682	50
1.5516	100

APPENDIX B: RAYLEIGH-BRILLOUIN SPECTRA

Rayleigh-Brillouin spectra in this sample had already been obtained as a by-product of the study of the depolarized Rayleigh scattering.[24] However, since the free spectral range (FSR) of the interferometer was optimized for this study (FSR=78 GHz), these spectra were of rather poor quality. At temperatures greater than 30° ($T-T_c>10°$) the Brillouin doublet was clearly in evidence (see Fig. 3) but its intensity could not be measured accurately because of the difficult evaluation of the background and of the Rayleigh wing. By using the same approximations for all spectra, the variation could be studied, and is reported in Fig. 4. The conclusion is that no background term in the Rayleigh line is visible and that Eq. (15) applies.

Therefore we recorded a single Rayleigh-Brillouin spectrum using a FSR of 5.92 GHz, at a temperature of 41.4 °C ($T-T_c\simeq21$ °C). For sake of brevity, we do not repeat the description of the setup which can be found in Ref. 25. The spectrum is shown in Fig. 5. Integration of the lines leads to a value

$$\frac{I_R}{2I_B}=30\ ,$$

while the Brillouin shift gives the speed of sound at this temperature,

$$v=1140\text{ m s}^{-1}\ .$$

The other parameters involved in Eq. (18) will be

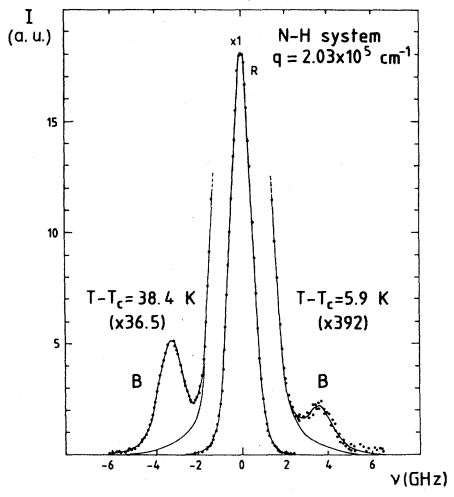

FIG. 3. Rayleigh-Brillouin spectrum recorded with a free spectral range of 78 GHz.

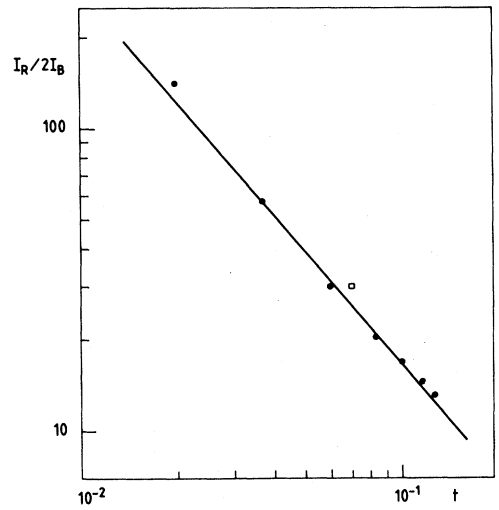

FIG. 4. Rayleigh-Brillouin ratio measured from spectra recorded with a FSR of 78 GHz, showing the pure power-law behavior. The square denotes the spectrum recorded with a FSR of 5.92 GHz.

discussed in the following appendixes.

We finally get

$$C_{\varphi}^{+}=(2.8\pm0.4)\times10^{-29}\ \mathrm{m}^3\ .$$

Or, using a more usual terminology,

$$\left[\frac{\partial\mu}{\partial\varphi}\right]_T=\frac{k_BT_c}{C_{\varphi}^{+}}=144\ \mathrm{J\,cm^{-3}}\ .$$

APPENDIX C: REFRACTIVE INDEX AND VOLUME MEASUREMENTS

As explained above, the specific heat was not directly measured. Instead we determined a change of density (or volume), taking advantage of the formula

$$C_{p,M}^{\mathrm{crit}}=-T_c\left[\frac{dT_c}{dp}\right]^{-1}\left[\frac{1}{\rho}\frac{\partial\rho}{\partial T}\right]_{p,M}^{\mathrm{crit}}=\frac{A^{+}}{\alpha}k_Bt^{-\alpha}\ . \tag{C1}$$

The density itself was deduced from refractive index and volume measurements.

1. Refractive index

The refractive index has been measured using the simple interferometer described and used in Ref. 26. The accuracy is of the order of magnitude of some 10^{-6} with the 2-cm sample length we used. The refractive indices of the pure components have been fitted to a linear variation:

$$n(T)-n(T_0)=\left[\frac{\partial n}{\partial T}\right]_p(T-T_0)$$

with $T_0\simeq T_c\simeq20\,^{\circ}\mathrm{C}$. The results of the fit are reported in Table IV.

The data of the mixture are reported in Table V and have been fitted according to (C1),

$$n(t)-n(t_0)=\left[\rho\frac{\partial n}{\partial\rho}\right]\left[\frac{dT_c}{dp}\right]k_B\frac{A^{+}}{\alpha}\int_{t_0}^{t}(t^{-\alpha}+\alpha a_c t^{\Delta-\alpha}+\cdots+\cdots)dt\ ,$$

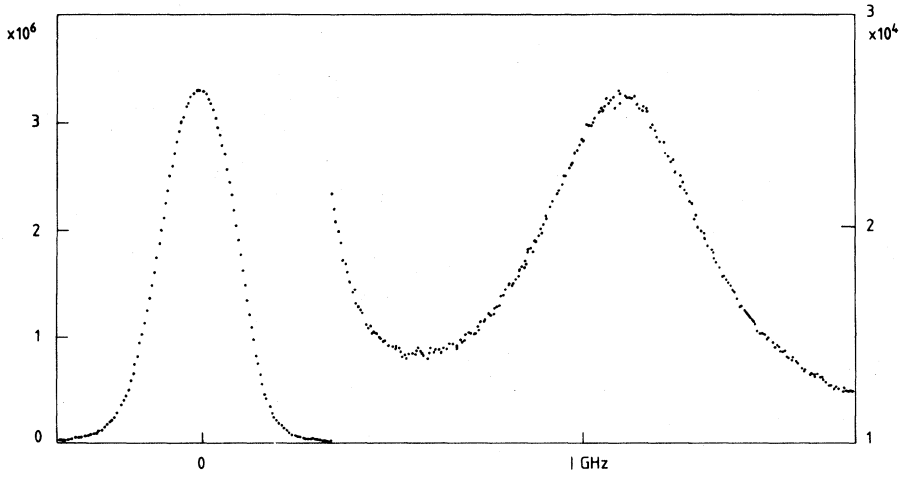

FIG. 5. Rayleigh-Brillouin spectrum recorded at 41.1 °C with a FSR of 5.92 GHz.

TABLE IV. Values of the parameters determined by refractive index and volume measurements (see text). Fits were performed to $\Delta n = T_c(\partial n/\partial T)^{\text{reg}}_{p,M} t + R_n t^{0.890}$ and $\Delta\rho = \rho T_c[(1/\rho)(\partial\rho/\partial T)^{\text{reg}}_{p,M}]t + R_\rho t^{0.890}$.

System	$n\left[\begin{matrix}6328\text{ Å}\\ 20\,^\circ\text{C}\end{matrix}\right]$	$\left[\frac{\partial n}{\partial T}\right]^{\text{reg}}_{p,M}$ (10^{-4} K^{-1})	$\alpha=0.110$ R_n (10^{-2})	20 °C ρ (10^3 kg m^{-3})	$\left[\frac{1}{\rho}\frac{\partial\rho}{\partial T}\right]^{\text{reg}}_{p,M}$ (10^{-4} °C^{-1})	$\alpha=0.110$ R_ρ (10^{-2})
Nitrobenzene	1.5480[a,b]	−4.827[c]± 0.005		1.2037[d]	−8.07±0.02[e]	
n-Hexane	1.3737[b]	−5.376[c]± 0.007		0.6603[d]	−12.60±0.06[f]	
Nitrobenzene	1.444[g]	−5.58± 0.04	1.16±0.09	0.8753[h] 0.8635[d]		
plus *n*-Hexane					(−11.82)[i]	2.79±0.08

[a]Reference 27.
[b]Cited in Ref. 28.
[c]This work. In order to obtain absolute values, add $+2.5\times10^{-7}$ K^{-1}, i.e., the correction due to the cell expansion.
[d]Cited in Ref. 22.
[e]This work. For absolute values, add 1% uncertainty and compare with $-(8.16\pm0.04)\times10^{-4}$ K^{-1} reported in d.
[f]This work. For absolute values, add 1% uncertainty and compare with $-(12.85\pm0.05)\times10^{-4}$ K^{-1} reported in d.
[g]This work.
[h]Ideal value.
[i]Value imposed to 1.08 times the ideal value. See text.

where the second ellipsis represents regular terms. In fact, no correction to scaling was found necessary and the data were well described by

$$n(t)-n(0)=T_c\left[\frac{\partial n}{\partial T}\right]^{\text{reg}}_{p,M} t + R_n t^{1-\alpha}\,.$$

The results are listed in Table IV, and the residuals of the fit are shown in Fig. 6. One can notice that the regular part

$$\left[\frac{\partial n}{\partial T}\right]^{\text{reg}}_{p,M} = 1.08\left[\frac{\partial n}{\partial T}\right]^{\text{id}}_{p,M},$$

where the ideal part is deduced from the pure components measurements,

$$\left[\frac{\partial n}{\partial T}\right]^{\text{id}} = -(5.177\pm0.007)10^{-4}\text{ K}^{-1}\,.$$

2. Volume measurements

In order to check that only the density is responsible for the critical behavior of the refractive index, we also performed volume measurements.

The dilatation of the mixture has been studied using the usual reservoir and capillary method. Owing to the small volume of the capillary a limited temperature range can be studied at a time ($\sim$2 K). An auxillary reservoir allowed us to adjust the amount of liquid without unsealing the cell. The pure components exhibited a linear expansion (see Table VI). The nonlinearity of the expansion of the mixture cannot be detected in a single temperature interval but the average slope changes with the mean temperature (see Fig. 7). These measurements are less precise than refractive index ones.

Therefore, it is impossible to deduce simultaneously the amplitude of the regular and singular parts. However, while the singular part of the refractive index might arise from a different process than the one of the density, this should not be the case for the regular part. So we imposed the regular part to be 1.08 times the ideal value as found in the refractive index data fit. The ratio of the singular to regular amplitudes for volume measurements is

TABLE V. Refractive index variations along the critical isochore.

First series		Second series	
t	Δn (10^3)	t	Δn (10^3)
6.06×10^{-2}	0	2.665×10^{-3}	0.004
5.31×10^{-2}	1.111	1.087×10^{-3}	0.242
4.51×10^{-2}	1.710	8.06×10^{-4}	0.272
4.908×10^{-2}	1.714	5.54×10^{-4}	0.307
3.998×10^{-2}	3.081	4.19×10^{-4}	0.326
3.173×10^{-2}	4.250	2.85×10^{-4}	0.342
3.174×10^{-2}	4.292	2.09×10^{-4}	0.351
2.445×10^{-2}	5.368	1.27×10^{-4}	0.361
1.902×10^{-2}	6.171	0.73×10^{-4}	0.367
1.384×10^{-2}	6.938	0.63×10^{-4}	0.376
1.086×10^{-2}	7.377		
1.085×10^{-2}	7.373		
7.703×10^{-3}	7.832		
6.323×10^{-3}	8.035		
5.506×10^{-3}	8.153		
4.609×10^{-3}	8.283		
3.353×10^{-3}	8.465		
2.749×10^{-3}	8.552		
2.174×10^{-3}	8.635		
1.599×10^{-3}	8.715		
1.033×10^{-3}	8.796		
7.512×10^{-4}	8.835		
4.71×10^{-4}	8.875		
1.93×10^{-4}	8.513		

1.13±0.15 times that found in refractive index measurements. This proves that the measured refractive index anomaly arises from the thermal expansion only. However, by comparing the changes in n and ρ, we can deduce

$$\rho\left[\frac{\partial n}{\partial \rho}\right]=(4.72\pm0.08)\times10^{-4}\ .$$

From the literature,[29] the shift of T_c with pressure is obtained

$$\left[\frac{\partial T_c}{\partial p}\right]=-(1.64\pm0.08)\times10^{-7}\ \mathrm{K\,Pa^{-1}}\ .$$

Hence we get

$$A_n^+=-\frac{\alpha(1-\alpha)}{k_B}\frac{R_n}{\rho\left[\frac{\partial n}{\partial \rho}\right]\left[\frac{\partial T_c}{\partial p}\right]}$$

$$=(1.05\pm0.15)\times10^{27}\ \mathrm{m^{-3}}\ .$$

TABLE VI. Dilatation of the nitrobenzene—n-hexane system near T_c. $T_c=19.522$ °C (add $+0.5$ °C to obtain absolute values).

T (°C)	Δx (cm)	T (°C)	Δx (cm)
Set 1		Set 4	
29.7125	4.575	19.7605	5.750
29.4330	3.780	19.6802	5.510
29.5660	4.160	19.5993	5.300
29.6998	4.530	19.5599	5.195
29.8340	4.895	19.5530	5.170
29.9693	5.275		
30.1079	5.645	Set 5	
30.2445	6.015	19.6304	5.330
30.3845	6.395	19.5484	5.130
30.5239	6.770	19.5330	5.085
30.6700	7.165	19.5514	5.125
30.8098	7.545	19.5690	5.155
30.9530	7.935	19.5845	5.205
		19.6102	5.260
Set 2		19.6434	5.335
23.0515	3.845	19.6824	5.445
23.1498	4.120	19.7153	5.525
23.2487	4.385	19.7575	5.630
23.3487	4.645	19.8413	5.820
23.4495	4.505	19.9260	6.050
23.5505	5.175	19.8271	5.805
23.6515	5.450	19.7429	5.590
23.8036	5.855	19.6601	5.395
23.9590	6.265	19.5786	5.180
24.1039	6.650	19.5465	5.100
24.2589	7.060	19.5306	5.060
24.4050	7.445	19.5443	5.080
24.5625	7.860		
Set 3			
20.3215	3.820		
20.4059	4.030		
20.5015	4.265		
20.6298	4.580		
20.7625	4.930		
20.8966	5.265		
21.0288	5.605		
21.1635	5.945		
21.2987	6.295		
21.4342	6.645		
21.5696	6.985		

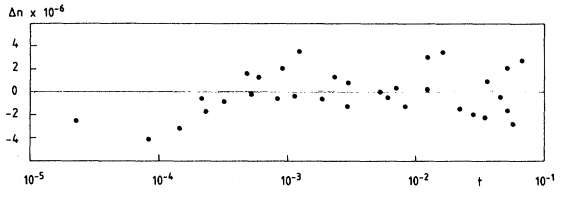

FIG. 6. Residuals of the fit of the refractive index along the critical isochore.

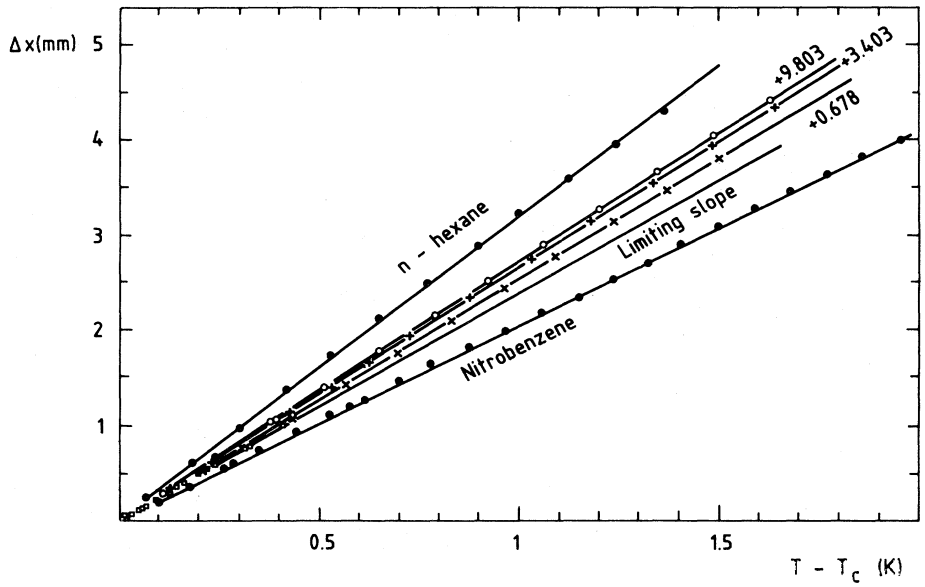

FIG. 7. Dilatation of the mixture at different temperatures observed by a volumetric method.

APPENDIX D: TURBIDITY MEASUREMENTS

The turbidity alone does not allow the determination of C^+, C^-, or C_c, but their product by the light scattering amplitude $(\partial n^2/\partial M)_{p,T}$, which is not a mere derivative and is not known. However, turbidity measurements can be useful in two different ways. The first is that close to the critical point the turbidity is also sensitive to the correlation length ξ. It is therefore an easy way to measure the correlation length amplitude since we know an ap-

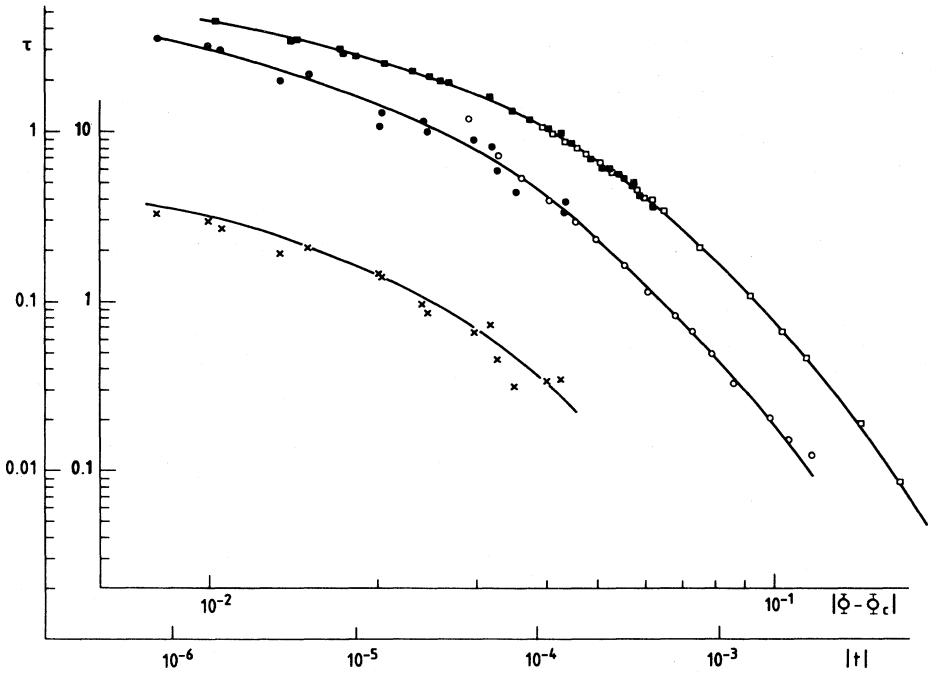

FIG. 8. Turbidity along the three principal trajectories. Critical isochore: ■, 5-mm cell; □, 2-cm cell. Coexistence curve: ●, 5-mm cell; ○, 2-cm cell. Critical isotherm: ×, 5-mm cell (inner scales). The $|\phi|$ and $|t|$ scales are related by $|\phi| = B|t|^{\beta}$.

TABLE VII. Coefficients of the approximation to Bray's structure factor [Eq. (A1)].

	a	$b=1-\mu$	c
1	1.040 056	$1-\frac{\eta}{2}=0.984\,25$	1
2	1.058 947	1.554 213	1
3	1.053 932	1.627 419	−1

propriate form of the correlation function.[14] The second is that the ratios of turbidity amplitudes do not depend on $(\partial n^2/\partial M)_{p,T}$ and that the ratios C^+/C^- or C^+/C_c can be directly measured. Turbidity measurements are straightforward: A light beam of constant intensity is sent through the mixture and the emergent intensity is measured. The original formulation of the correlation function being very cumbersome, an approximation valid within 1% has been worked out[19,23]:

$$G(k\xi)=\sum_{i=1}^{3} C_i(1+a_i^2k^2\xi^2)^{-b_i}$$

which can readily be integrated over angles to give

$$\begin{aligned}G'(X_0)=\sum_{i=1}^{3} c_i\{&[(1+2a_i^2X_0^2)^{\mu_i}-1]\\&\times[1+a_i^2X_0^2(2-\mu_i)\\&+a_i^4X_0^4(2+\mu_i+\mu_i^2)]\\&-2\mu_i a_i^2X_0^2(1+a_i^2X_0^2)\}\\&\times[a_i^6X_0^6\mu_i(1+\mu_i)(2+\mu_i)]^{-1}\end{aligned}$$

with $X_0=\sqrt{2}k_0\xi$. The a_i's are given in Table VII. The turbidity has to be fitted to the function

$$\tau=\frac{2\pi^3}{\lambda_0^4}S_n^2\left[\frac{\partial n^2}{\partial\varphi}\right]^2(1+t)C_\varphi^i t^{-\gamma}G'(\sqrt{2}k_0\xi^i)\ ,$$

TABLE VIII. Turbidity along the critical isochore.

t	τ (cm^{-1})	t	τ (cm^1)
$l=2$ cm		$l=0.5$ cm	
9.74×10^{-3}	8.7×10^{-3}	2.20×10^{-4}	6.05×10^{-1}
5.88×10^{-3}	1.91×10^{-2}	2.20×10^{-4}	6.05×10^{-1}
2.90×10^{-3}	4.61×10^{-2}	1.89×10^{-4}	6.88×10^{-1}
2.17×10^{-3}	6.60×10^{-2}	1.88×10^{-4}	6.88×10^{-1}
1.44×10^{-3}	1.08×10^{-1}	1.52×10^{-4}	8.41×10^{-1}
7.54×10^{-4}	2.09×10^{-1}	1.52×10^{-4}	8.64×10^{-1}
4.81×10^{-4}	3.40×10^{-1}	1.52×10^{-4}	8.64×10^{-1}
4.16×10^{-4}	3.93×10^{-1}	1.32×10^{-4}	9.58×10^{-1}
3.75×10^{-4}	4.04×10^{-1}	1.09×10^{-4}	1.03×10^{0}
3.45×10^{-4}	4.39×10^{-1}	1.08×10^{-4}	1.06×10^{0}
2.49×10^{-4}	5.69×10^{-1}	8.91×10^{-5}	1.16×10^{0}
2.15×10^{-4}	6.37×10^{-1}	8.84×10^{-5}	1.16×10^{0}
1.81×10^{-4}	7.24×10^{-1}	7.20×10^{-5}	1.30×10^{0}
1.60×10^{-4}	7.88×10^{-1}	7.10×10^{-5}	1.30×10^{0}
1.90×10^{-4}	8.62×10^{-1}	5.36×10^{-5}	1.54×10^{0}
1.19×10^{-4}	9.59×10^{-1}	5.29×10^{-5}	1.54×10^{0}
1.06×10^{-4}	1.04×10^{0}	3.24×10^{-5}	1.33×10^{0}
		3.17×10^{-5}	1.86×10^{0}
$l=0.5$ cm		2.87×10^{-5}	1.97×10^{0}
4.22×10^{-4}	3.41×10^{-1}	2.80×10^{-5}	1.97×10^{0}
4.21×10^{-4}	3.59×10^{-1}	2.53×10^{-5}	2.10×10^{0}
3.53×10^{-4}	4.31×10^{-1}	2.08×10^{-5}	2.18×10^{0}
3.52×10^{-4}	4.31×10^{-1}	2.05×10^{-5}	2.22×10^{0}
3.23×10^{-4}	4.88×10^{-1}	1.43×10^{-5}	2.52×10^{0}
3.22×10^{-4}	4.68×10^{-1}	9.90×10^{-6}	2.74×10^{0}
2.93×10^{-4}	5.26×10^{-1}	9.56×10^{-6}	2.74×10^{0}
2.92×10^{-4}	5.26×10^{-1}	8.53×10^{-6}	2.93×10^{0}
2.67×10^{-4}	5.46×10^{-1}	8.19×10^{-6}	2.99×10^{0}
2.67×10^{-4}	5.46×10^{-1}	4.78×10^{-6}	3.36×10^{0}
2.45×10^{-4}	5.64×10^{-1}	4.44×10^{-6}	3.36×10^{0}
2.45×10^{-4}	5.84×10^{-1}	1.71×10^{-6}	4.38×10^{0}

TABLE IX. Turbidity along the coexistence curve.

$\|t\|$	τ (cm^{-1})
$l=2$ cm	
9.27×10^{-3}	2.54×10^{-3}
3.12×10^{-3}	1.29×10^{-2}
2.33×10^{-3}	1.55×10^{-2}
1.86×10^{-3}	2.07×10^{-2}
1.15×10^{-3}	3.30×10^{-2}
8.70×10^{-4}	4.96×10^{-2}
6.69×10^{-4}	6.96×10^{-2}
5.36×10^{-4}	8.26×10^{-2}
4.03×10^{-4}	1.15×10^{-1}
2.90×10^{-4}	1.64×10^{-1}
2.08×10^{-4}	2.36×10^{-1}
1.60×10^{-4}	2.90×10^{-1}
1.16×10^{-4}	3.86×10^{-1}
$l=0.5$ cm	
1.40×10^{-4}	3.92×10^{-1}
1.33×10^{-4}	3.52×10^{-1}
7.40×10^{-5}	4.52×10^{-1}
5.95×10^{-5}	5.71×10^{-1}
5.51×10^{-5}	8.10×10^{-1}
4.38×10^{-5}	8.91×10^{-1}
2.50×10^{-5}	1.01
2.26×10^{-5}	1.15
1.38×10^{-5}	1.27
1.32×10^{-5}	1.07
5.46×10^{-6}	2.15
3.86×10^{-6}	1.93
1.82×10^{-6}	3.01
1.52×10^{-6}	3.21
8.23×10^{7}	3.51

where the superscript i denotes the trajectory ($i=+,-,C$).

Since the reference cell was not exactly critical, it could not provide accurate data close to the critical point, which are important for the determination of the correlation length. Therefore we also used data from a variable concentration cell, the optical path of which was 0.5 cm. The range in concentration spanned was $\phi=(\pm4.2\times10^{-2})$ and data were taken from above the critical isotherm down to the coexistence curve. These data are a by-product of a nonequilibrium experiment.[30]

We fitted together both series for the critical isochore and the coexistence curve (see Tables VIII and IX and Fig. 8) and got

$$S_n^2C_\varphi^+=(2.45\pm0.04)\times10^{-29}\ \text{m}^3\ ,$$

$$S_n^2C_\varphi^-=(0.58\pm0.02)\times10^{-29}\ \text{m}^3\ ,$$

$$\xi_0^+=(2.65\pm0.07)\times10^{-10}\ \text{m}\ ,$$

$$\xi_0^-=(1.4\pm0.1)\times10^{-10}\ \text{m}\ .$$

TABLE X. Turbidity along the critical isotherm.

$\|\phi-\phi_c\|$	τ (cm^{-1})
4.22×10^{-2}	0.39
4.03×10^{-2}	0.33
3.50×10^{-2}	0.31
3.28×10^{-2}	0.45
3.18×10^{-2}	0.73
2.96×10^{-2}	0.65
2.46×10^{-2}	0.85
2.38×10^{-2}	0.93
2.03×10^{-2}	1.39
2.00×10^{-2}	1.43
1.50×10^{-2}	2.11
1.34×10^{-2}	1.91
1.05×10^{-2}	2.7
0.99×10^{-2}	2.95
0.81×10^{-2}	3.3

The data can also be interpolated at the critical temperature, providing a way of determining both D and ξ_0^c (see Table X). The analysis is the same, provided we replace t by $(M/B)^{1/\beta}$. We therefore get (instead of $S_n^2C^\pm$)

$$S_n^2(\delta DB^{\delta-1})^{-1}=(0.29\pm0.05)\times10^{-29}\ \text{m}^3$$

(instead of $\xi_0^\pm$)

$$\xi_0^c(BD^{1/\delta})^{-\nu/\beta}=(0.93\pm0.10)\times10^{-10}\ \text{m}\ .$$

APPENDIX E: CORRELATION TIME MEASUREMENTS

Spectral measurements of the Rayleigh line in this sample had already been obtained. However, we felt the need of more precise data. We used for that a clipped photon correlator (ATNE). The scattering angle was 90° and the incident radiation was issued from a small power He-Ne laser ($\lambda=632.8$ nm). No departure from an exponential decay was noticed. The correlation times are re-

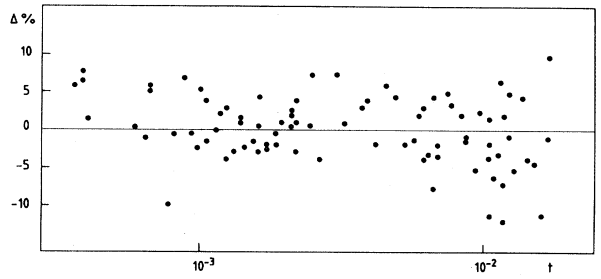

FIG. 9. Residuals of the fit of the linewidth data to the Kawasaki function with $R=0.99$.

TABLE XI. Correlation time of the concentration fluctuations along the critical isochore.

t	τ (μs)	t	τ (μs)
5.52×10^{-3}	48.1	2.87×10^{-3}	66.7
5.91×10^{-3}	47.1	2.62×10^{-3}	80.3
6.31×10^{-3}	44.8	2.38×10^{-3}	75.5
6.71×10^{-3}	42.2	2.372×10^{-3}	81.6
7.12×10^{-3}	37.7	2.120×10^{-3}	84
8.02×10^{-3}	35.8	2.120×10^{-3}	87.2
9.46×10^{-3}	31.8	2.120×10^{-3}	91.2
1.081×10^{-2}	31.9	1.864×10^{-3}	96
1.2×10^{-2}	27.9	1.604×10^{-3}	107.6
1.2×10^{-2}	27.9	1.413×10^{-3}	112
1.588×10^{-2}	22.7	1.413×10^{-3}	115.2
1.614×10^{-2}	19.8	1.215×10^{-3}	118.4
1.540×10^{-2}	25.9	1.215×10^{-3}	128
1.467×10^{-2}	25.1	1.027×10^{-3}	136
1.409×10^{-2}	25.6	1.027×10^{-3}	128
1.328×10^{-2}	24.3	8.43×10^{-4}	137.6
1.247×10^{-2}	28.4	6.59×10^{-4}	156.8
1.165×10^{-2}	30.4	6.55×10^{-4}	157.4
1.165×10^{-2}	32	3.69×10^{-4}	192.8
1.165×10^{-2}	27.5	3.69×10^{-4}	193.3
1.084×10^{-2}	30.7	3.69×10^{-4}	196
1.084×10^{-2}	27.6	5.80×10^{-4}	176.7
1.084×10^{-2}	27.5	3.99×10^{-4}	203.4
1.003×10^{-2}	35.2	7.61×10^{-4}	173.5
1.003×10^{-2}	32	9.42×10^{-4}	141.4
1.003×10^{-2}	30.9	1.120×10^{-3}	128.5
9.22×10^{-3}	35.2	9.45×10^{-4}	144.5
9.22×10^{-3}	28.7	1.304×10^{-3}	121.6
8.40×10^{-3}	36	1.355×10^{-3}	113.6
7.59×10^{-3}	36.6	1.492×10^{-3}	110.8
6.47×10^{-3}	40.3	1.672×10^{-3}	104
6.47×10^{-3}	46.2	1.857×10^{-3}	97.6
1.202×10^{-2}	26.0	2.041×10^{-3}	90
1.008×10^{-2}	32.5	2.044×10^{-3}	88
8.38×10^{-3}	36	2.041×10^{-3}	88.3
6.83×10^{-3}	42.4	3.672×10^{-3}	60
6.02×10^{-3}	43.2	2.041×10^{-3}	88
6.02×10^{-3}	43.2	1.501×10^{-3}	93.2
5.70×10^{-3}	45.3	1.727×10^{-3}	102.4
5.06×10^{-3}	51.2	1.553×10^{-3}	101.2
4.73×10^{-3}	49.8	1.553×10^{-3}	106
4.42×10^{-3}	51.2	1.345×10^{-3}	114.4
4.09×10^{-3}	59.2	1.164×10^{-3}	122
3.77×10^{-3}	58.4	9.50×10^{-4}	129.1
3.44×10^{-3}	67.5	8.09×10^{-4}	153
3.36×10^{-3}	61.0	6.28×10^{-4}	173.2
3.12×10^{-3}	68.3	3.58×10^{-4}	199.6

ported in Table XI. The data are in very good agreement with those of Ref. 31.

They have been fitted to both the Kawasaki equation (24) (see Fig. 9) and Peliti-Paladin formulas, using the value of ξ_0 determined by turbidity measurements. The viscosity was determined in Ref. 32. However, a later check of the calibration of the viscosimeter revealed a 5% systematic error on the absolute values. The viscosity has therefore been calculated using

$$\eta = \eta_0 \exp\left[\frac{E}{1+t}\right] t^{-y_\eta}$$

with $\eta_0 = 1.36 \times 10^{-4}$ P, $E = 3.58$, and $y_\eta = 0.043$. The only adjustable parameter was R. Since most of the data lie in the hydrodynamic region, the functions are very close to each other. Therefore, the values obtained,

$$R_K = 0.99 \pm 0.05 ,$$

$$R_{PP} = 0.98 \pm 0.05 ,$$

are very close to each other. The uncertainty includes the error on ξ_0 and q.

---

*Permanent address: Ecole Normale Supérieure, 43 rue de la Liberté, Le Bardo, Tunisie.

[1]F. J. Wegner, Phys. Rev. B 5, 4529 (1972).
[2]For review, see *Phase Transitions, Status of the Experimental and Theoretical Situation,* edited by M. Lévy, S. C. le Guillou, and J. Zinn-Justin (Plenum, New York, 1981).
[3]E. Brézin, J. C. le Guillou, and J. Zinn-Justin, Phys. Lett. 47A, 285 (1974).
[4]H. B. Tarko and M. E Fisher, Phys. Rev. B 11, 1217 (1975).
[5]A. Aharony and P. C. Hohenberg, Phys. Rev. B 13, 3081 (1976).
[6]C. Bervillier, Phys. Rev. B 14, 73 (1976).
[7]D. Stauffer, M. Ferer, and M. Wortis, Phys. Rev. Lett. 29, 345 (1972).
[8]D. Beysens, J. Chem. Phys. 64, 2579 (1976).
[9]Y. Garrabos, G. Zalczer, and D. Beysens, Phys. Rev. A 25, 1147 (1982).
[10]D. Beysens and A. Bourgou, Phys. Rev. A 19, 2407 (1979).
[11]J. V. Sengers, D. Bedeaux, P. Mazur, and S. C. Greer, Physica (Utrecht) 104A, 573 (1980) and references therein.
[12]D. Beysens and M. Gbadamassi, Phys. Rev. Lett. 47, 846 (1981).
[13]P. Calmettes, I. Lagues, and C. Laj, Phys. Rev. Lett. 28, 478 (1972).
[14]A. J. Bray, Phys. Rev. B 14, 1248 (1976).
[15]K. Kawasaki, Ann. Phys. (N.Y.) 61, 1 (1970).
[16]R. A. Ferrell, Phys. Rev. Lett. 24, 1169 (1970).
[17]E. D. Siggia, B. I. Halperin, and P. C. Hohenberg, Phys. Rev. B 13, 2110 (1976).
[18]H. C. Burstyn and J. V. Sengers, Phys. Rev. A 25, 448 (1982).
[19]D. Beysens, in Ref. 1.
[20]C. Paladin and L. Peliti, J. Phys. Lett. 43, L15 (1982).
[21]S. H. Chen and N. Polonski, Opt. Commun. 1, 64 (1969).
[22]J. Timmermans, in *Physico Chemical Constants of Pure Organic Compounds* (Elsevier, Amsterdam, 1965).
[23]D. Beysens, A. Bourgou, and P. Calmettes, Saclay Report No. DPhG/PSRM/1538/81 (unpublished).
[24]D. Beysens and G. Zalczer, Phys. Rev. A 18, 2280 (1980).
[25]D. Beysens and G. Zalczer, Opt. Commun. 23, 142 (1977).
[26]D. Beysens, Rev. Sci. Instrum. 50, 509 (1979).
[27]D. Beysens and P. Calmettes, J. Chem. Phys. 66, 766 (1977).
[28]Landolt-Boïnstein, in *Eigenshaften de Materie. . .8-Teil Optische Konstanten* (Springer, Berlin, 1962).
[29]J. Timmermans, *The Physico-Chemical Constants of Binary Systems in Concentrated Solutions* (Interscience, New York, 1959).
[30]D. Beysens, M. Gbadamassi, and M. Bouanz (unpublished).
[31]D. Beysens and G. Zalczer, Phys. Rev. A 15, 765 (1977).
[32]D. Beysens, S. H. Chen, J. P. Chabrat, L. Letamendia, J. Rouch, and C. Vaucamps, J. Phys. (Paris) Lett. 38, 203 (1977).